NIH Public Access
Author Manuscript
Nanomedicine. Author manuscript; available in PMC 2012 June 1.

Published in final edited form as:
Nanomedicine. 2011 June ; 7(3): 249–258. doi:10.1016/j.nano.2010.09.002.

Luminescence targeting and imaging using a nanoscale generation 3 dendrimer in an *in vivo* colorectal metastatic rat model

Marco A. Alcala, MD[1], **Shu Ying Kwan, BS**[4], **Chad M. Shade, MS**[3], **Megan Lang, BS**[5], **Hyounsoo Uh, MS**[3], **Manyan Wang, MS**[3], **Stephen G. Weber, PhD**[3], **David L. Bartlett, MD**[1], **Stéphane Petoud, PhD**[3,6,7], and **Yong J. Lee, PhD**[1,2,7]

[1]Department of Surgery, University of Pittsburgh School of Medicine, Pittsburgh, PA 15213, USA

[2]Department of Pharmacology & Chemical Biology, University of Pittsburgh School of Medicine, Pittsburgh, PA 15213, USA

[3]Department of Chemistry, University of Pittsburgh, Pittsburgh, PA 15260, USA

[4]Department of Biological Sciences, Carnegie Mellon University, Pittsburgh, PA 15213, USA

[5]Center for Biological Imaging, University of Pittsburgh, PA 15261, USA

[6]Centre de Biophysique Moléculaire, CNRS UPR 4301, rue Charles Sadron, 45071 Orléans, France

Abstract

Surgery is currently the best approach for treating either primary or metastatic hepatic malignancies. Since only 20% of patients with hepatic cancer are operable, regional therapies (RT) are emerging as alternate treatment modalities. However, RT's can have their own limitations at controlling tumor growth or lack the ability to detect such metastases. More can be done to enhance their efficacy. An animal model of hepatic metastases coupled with a gastroduodenal artery (GDA) cannulation technique may provide a site to apply such therapies. In our study, splenic injections were performed with CC531 adenocarcinoma cells, which generated metastatic hepatic tumors in WAG/RijHsd rats. Cannulation of GDA was achieved via a polyethylene catheter. Infusion of generation 3 polyamidoamine 4-amino-1,8-naphthalimide containing 8 europium ions (Eu-G3P4A18N) dendrimer via the GDA resulted in luminescence of the hepatic metastatic nodules. Imaging of the metastatic hepatic nodules was obtained with the help of a digital charge coupled device camera.

Keywords

dendrimer; imaging; targeting; hepatic metastatic model

© 2010 Elsevier Inc. All rights reserved

Corresponding Authors: Dr. Yong J. Lee, Department of Surgery, University of Pittsburgh, The Hillman Cancer Center, 5117 Centre Ave., Pittsburgh, PA 15213, U.S.A. Tel (412) 623-3268; Fax (412) 623-7709; leeyj@upmc.edu.. Prof. Stéphane Petoud, CNRS UPR4301, Centre de Biophysique Moléculaire, CNRS, rue Charles Sadron, 45071 Orléans, France. Tel +33 (0)2 38 26 56 52; Fax: +33 (0)2 38 63 15 17; stephane.petoud@cnrs-orleans.fr.
[7]Corresponding authors share primary corresponding authorship.

Publisher's Disclaimer: This is a PDF file of an unedited manuscript that has been accepted for publication. As a service to our customers we are providing this early version of the manuscript. The manuscript will undergo copyediting, typesetting, and review of the resulting proof before it is published in its final citable form. Please note that during the production process errors may be discovered which could affect the content, and all legal disclaimers that apply to the journal pertain.

Conflict of interest statement: The authors declare that there are no conflicts of interest.

NIH-PA Author Manuscript
NIH-PA Author Manuscript
NIH-PA Author Manuscript

NIH-PA Author Manuscript

NIH-PA Author Manuscript

NIH-PA Author Manuscript

Background

The liver is the most common site of distant metastases of colorectal cancer. About 150,000 Americans are diagnosed with colorectal cancer each year and about 50,000 of them will die from metastases of this disease.1 Approximately 50% of patients with colorectal cancer develop metastatic liver disease, of these patients, only 20% are operable. Once liver metastases have occurred, the patient's prognosis declines to a 5 year survival rate of 5%.2 For operable patients, surgery is the best treatment for liver metastases when compared to the available regional therapies such as radiofrequency ablation,3 transarterial chemoembolization (TACE) or radiation, resulting in a 5 year survival rate of 30%. Survival to five years is 5–9% in patients with unresected hepatic metastases who have received only conventional systemic chemotherapy.4 Some of the current therapies include local tumor ablation (i.e., applying alcohol or acetic acid directly into the metastatic lesions, cryotherapy or radiofrequency ablation), isolated hepatic perfusion, TACE and external radiation therapy. To better treat patients with inoperable liver metastases, current regional therapies need to be better understood and their efficacy need to be improved by being able to combine detection and treatment functions.

The survival studies in our rat model have allowed us to use a cannulation technique in which to deliver our functionalized dendrimer. Several studies have developed rat models of liver metastases[5], [6], and [7] but the surgical techniques were not adequately detailed. Gupta et al, described a liver infusion model by cannulating through the GDA with catheter placement into the hepatic artery.8 Others have also described directly cannulating the hepatic artery9 as well as the portal vein.10 The approach described here allows the main blood supply to the liver to be spared from trauma and the GDA to be ligated, mimicking the clinical application of RT's where isolated hepatic perfusion is initiated via the GDA. We are now reporting an *in vivo* hepatic colorectal metastases rat model via splenic injections with CC531 colorectal cancer cells. Previous studies have shown that colorectal metastases can be initiated by injecting cancer cells via the portal vein and superior mesenteric vein.11 These approaches lead to small diffuse lesions in the liver.12 In this study, we chose the splenic injection method. Metastasis by way of injecting the spleen has allowed us to mimic more closely the clinical patient and study a more relevant model.

The field of polymer chemistry has enabled the development of dendrimer nanotechnology for application in cancer therapy.[13], [14], and [15] Polycationic polymers such as poly(lysine)s, poly(ethylene-imine)s, diethylaminoethyl dextrans, and polyamidoamine (PAMAM) dendrimers have demonstrated great potential for application in cancer therapy. Through the iterative coupling of dendrons (the monomer of dendrimers) versatile “carrier devices” on the nanometer scale can be synthesized. Dendrimers are built from successive layers or generations of dendron coupling, so the diameters grow linearly while the number of coordinating groups grows geometrically. This characteristic allows for a concentration of various types of metal ions within a discrete dendrimer, offering the advantage of a relatively small but dense functional molecule.16 PAMAM dendrimers have shown good biocompatibility and *in vivo* deliverability without significant degradation.[17] and [18] The branch termini of the PAMAM family of dendrimers contain chemical groups such as terminal primary amines, alcohol or carboxylic groups that enable the dendrimers to be functionalized with suitable groups such as 1,8-naphthalimide chromophores to serve as photon emitters, or targeting molecules. In this study, we used a novel dendrimer, which we have developed, that incorporates generation-3 (G3) PAMAM with derivatives of 1,8-naphthalimide groups covalently substituted on all thirty-two terminal groups. Eight Eu^{3+}cations were encapsulated within the available binding sites present along the interior branches of each dendrimer, resulting in robust luminescent probes which possess maximum

NIH-PA Author Manuscript

NIH-PA Author Manuscript

NIH-PA Author Manuscript

signal intensity per unit volume. Our studies reveal that this new dendrimer Eu-G3P4A18N, which contains 8 europium ions, can become luminescent for imaging studies in order to detect the distribution sites of metastatic hepatic colorectal tumors in our *in vivo* rat model.

Methods

Animal model

Four to six week old male WAG/RijHsd rats were purchased from Harlan, Netherlands. Rats were fed ad libitum and maintained in environments with controlled temperature of 22–24°C and 12 hours light and dark cycles. All procedures involving the rats were in accordance with the Guide for the Care and Use of Laboratory Animals (National Research Council, 1996) and on a protocol approved by the Institutional Animal Care and Use Committee of the University of Pittsburgh.

Cell culture and generation of colorectal metastasis by splenic injection

CC531 cell line is a moderately differentiated colon adenocarcinoma syngeneic to WAG/RijHsd rats. Tumor cells were tested and found to be virus- and mycoplasma-free. CC531 cells were cultured in Dulbecco's modified eagle medium (DMEM) (Gibco; Grand Island, NY, USA) supplemented with 10% fetal bovine serum. Cells were maintained by serial passage. Tumor cells were harvested with a solution of 0.25% trypsin (Sigma; St. Louis, MO, USA), washed three times in 0.9% NaCl solution buffered with 1.4 mM phosphate (PBS) and adjusted to a suspension containing 2×10^6 viable (trypan blue exclusion test) tumor cells per 200 μL of PBS, which were then injected into the spleen to generate metastatic tumor nodules in the liver.

Metastatic lesions to the liver were revealed 15–20 days later after a midline incision was performed. Figures 1A and 1B both show the metastatic nodules in a rat liver after two and four weeks, respectively.

Anesthesia

Rats were anesthetized with a single intraperitoneal injection of 70 mg/kg of Ketamine (Bedford Labs, Ohio, USA) and 2.5 mg/kg of Acepromazine (Boehringer Ingleheim Vetmedica, Inc., MO, USA). An intramuscular injection of 0.1 mg/kg of buprenorphine (Bedford Labs, Ohio, USA) was also administered for analgesia prior to incision and 12–24 hours later if rats displayed any sign of distress.

GDA cannulation procedure with Eu-G3P4A18N (generation 3 polyamidoamine 4-amino-1,8-naphthalimide containing 8 europium ions)

Once anesthetized, the rat was placed in the supine position on a heating pad (Deltaphase Isothermal Pad, Braintree Scientific, Mass, USA) to maintain body temperature. The abdomen was shaved and sterilely prepared; all subsequent steps were performed aseptically; non-glare bright lighting was obtained with a fiber optic light source (Ehrenreich Photo Optical Industries, NY, USA). A 5 cm midline incision was made using a #10 scalpel and carried down into the peritoneal cavity and hemostasis was achieved with sterile gauze and pressure. The bowel was then brought to the surface and flipped to the left of the abdomen revealing the hepaticoduodenal ligament, portal vein, hepatic artery, bile duct and inferior aspect of the liver. The portal vein was isolated using a 6-0 silk suture and fine tipped tweezers (Miltex, Pennsylvania, USA) were used to reveal the vein, allowing clear visualization of the hepatic artery running posterior and adherent to it. After the hepatic artery was separated from the portal vein, the artery was then isolated with a 6-0 silk suture (Figure 2A). The hepatic artery was traced inferiorly to the branching point where it meets with the GDA. The GDA was also isolated using a 6-0 silk suture at the most inferior point

NIH-PA Author Manuscript

NIH-PA Author Manuscript

NIH-PA Author Manuscript

and skeletonized using fine tipped tweezers. Two 6-0 silk sutures were placed about 3 mm apart at the superior portion of the GDA and tied on loosely for control of the catheter after placement (Figure 2A). Fine tipped 4.5 inch curved iris scissors (Miltex, Pennsylvania, USA) were used to make a 0.5 mm arteriotomy into the middle of the GDA without bisecting it. Hemostasis was achieved with the superiorly placed 6-0 silk sutures. A 30 gauge needle bent halfway was used as a "hook" to help guide a polyethylene (PE-10) catheter (Becton, Dickinson and Company, New Jersey, USA) retrograde into the GDA and placed just before the bifurcation of the hepatic artery and the GDA (Figure 2B). The catheter was inserted into the arteriotomy and placed approximately 4 mm into the GDA, stopping before the GDA-hepatic artery junction. The superiorly placed suture along with a second one placed 1 mm next to it was tied down to secure the catheter (Figure 2A).

To prevent inflow of blood into the liver, micro vessel clamps were placed on the portal vein and the hepatic artery (Figure 2C). Catheter placement was confirmed by visualizing blood return in the catheter upon drawing back on the syringe and patency was confirmed with an infusion of 1–2 ml of normal saline. Complete isolation of the liver was achieved through occlusion of the suprahepatic inferior vena cava (IVC) with cotton swabs during infusion of Eu-G3P4A18N.

Synthesis of Eu-G3P4A18N

Glycine-conjugated 4-amino-1,8-naphthalimide was synthesized by a reported method.19 Glycine-conjugated 4-amino-1,8-naphthalimide was attached on the amine-terminated G3 PAMAM dendrimer by a standard amide coupling condition: 54.1 mg (2.00×10^{-4} mol) of glycine-naphthalimide conjugate was added to a solution of 29.4 mg (4.26×10^{-6} mol) of G3 PAMAM dendrimer (Dendritech Inc.; Midland, MI, USA) in 5 mL of DMF (dimethylformamide) (Sigma-Aldrich; St. Louis, MO, USA). 92.1 mg (2.42×10^{-4} mol) of HATU (2-(1H7-7-Azabenzotriazol-1-yl)-1,1,3,3-tetramethyl uranium hexafluorophosphate Methanaminium) (Aldrich; St. Louis, MO, USA) and 70 μL (52 mg; 4.0×10^{-4} mol) of DIPEA (*N*,*N*-Diisopropylethylamine) (Sigma-Aldrich; St. Louis, MO, USA) were added (Figure 3A). The reaction mixture was stirred at room temperature for two days under nitrogen atmosphere while monitoring for the disappearance of G3 PAMAM dendrimer by TLC (thin layer chromatography). The compound was purified by dialysis using a regenerated cellulose membrane (nominal molecular weight cut-off (MWCO) 12,000–14,000; Fisher Scientific; Pittsburgh, PA, USA) in dimethyl sulfoxide (DMSO) for three days. The solution recovered from the dialysis membrane was dried in a vacuum oven (40°C, 50 mbar) to yield G3P4A18N as brown solid (52.5 mg, 82%). G3P4A18N was characterized by ^{1}H-NMR (nuclear magnetic resonance) (300 MHz, DMSO-d_6) (Figure 3B): δ 8.54 p.p.m. (br s, 32 H), 8.32 (br s, 32 H), 8.15 (br s, 32 H), 8.10 (br s, 32 H), 7.90 (br s, 32 H), 7.76 (m, 28 H), 7.56 (br s, 32 H), 7.40 (br s, 64 H), 6.78 (br s, 32 H), 4.56 (br s, 64 H), 3.08 (m, 184 H), 2.61 (m, 120 H), 2.39 (m, 60 H), 2.16 (m, 120 H); analysis (% calcd, % found for $C_{750}H_{864}N_{186}O_{156}\cdot 32DMSO\cdot 64H_2O$): C (52.47, 51.74), H (6.40,6.29), N (13.98, 13.76). The Eu^{3+} complex of G3P4A18N (Eu-G3P4A18N) was synthesized by the following method adapted from one of our methods:20 22.67 mg (1.513×10^{-6} mol) of G3P4A18N (generation 3 polyamidoamine 4-amino-1,8-naphthalimide) was dissolved in 10 mL of DMSO. 647.5 μL of 18.7 mM $Eu(NO_3)_3$ solution in DMSO (1.21×10^{-5} mol) was added to the dendrimer solution. Formation of Eu^{3+} complexes with the G3 PAMAM dendrimer was confirmed as described previously.20 The mixture was diluted to 25.00 mL and incubated at room temperature for seven days. The resulting solution (conc. = 60.5 μM) was used as obtained and the final configuration is seen in Figure 3C.

NIH-PA Author Manuscript

NIH-PA Author Manuscript

NIH-PA Author Manuscript

Luminescence of Eu-G3P4A18N

As explained above, we have developed the synthesis of Eu-G3P4A18N dendrimer. The absorption and emission spectra of this dendrimer were measured (data not shown). The absorption spectrum displays a maximum at approximately 440 nm. The fluorescence emission spectrum displays a prominent band with an intensity maximum at 555 nm. For the photobleaching experiment (Figure 3D), Eu-G3P4A18N dendrimer and its control G3P4A18N dendrimer at 10 μM were sealed in capillary tubes to minimize effects from solvent evaporation and diffusion. Each sample was focused in an IX81 inverted fluorescence microscope (Olympus, Melville, NY, USA) coupled with a cooled charge coupled device (CCD) (ORCA-ER High Resolution Digital B/W CCD Camera, B&B Microscopes Limited, Pittsburgh, PA, USA). A Cermax® 300 W Xenon Arc lamp (PE300BF, PerkinElmer Optoelectronics, Fremont, CA, USA) in the microscope was used as the excitation source (dry 40× NA 0.95 UPlanSAPO objective lens from Olympus). Image processing was performed by the image acquisition software SimplePCI from Compix Inc (Sewickley, PA, USA). A fluorescence cube DAPI EX D350/50X BS400 EM460/50) filter was used for the experiments, exposing a 40× selected area with the xenon lamp. Transmittance spectra of the excitation and emission filters were used in the photobleaching experiment.

Luminescence imaging of hepatic tumors

The luminescence of Eu-G3P4A18N (300μL of a 60μM solution in 10% DMSO/H_2O) was captured while selectively associating with the liver tumors. The imaging system used to detect the luminescence of the dendrimer is custom-made, combining either an Andor DU 434-BR-DD cooled charge coupled device (CCD) camera (Andor Technology; South Windsor, Connecticut, USA) or a Rolera XR fast digital CCD camera (QImaging; Surrey, Canada) fitted with a 50 mm AF Nikkor lens containing a minimum aperture of F16 and maximum aperture of F1.4. The emission filter used was 610/30 nm (Chroma Technologies; Bellows Falls, VT, USA). The rat livers on living animals were excited using four 450 nm emitting 5 W LEDs (Lumileds Lighting; San Jose, CA, USA). Qcapture software (QImaging; Surrey, Canada) was used for the data acquisition.

Histopathology of liver tumor sections

Tissue sections (10 microns) from dendrimer-infused livers were also processed for immunohistochemistry staining. Tissues were fixed with 2% paraformaldehyde for 2 hour at 4°C, and then left overnight in 30% sucrose at 4°C. The samples were frozen in a liquid nitrogen-cooled bath of 2-methyl-butane and cryosectioned. Sections were labeled with monoclonal CD31 (ABR MA1-26196) and Alexa Fluor 647 phalloidin (Invitrogen A22287). The application of goat anti mouse Cy3 secondary antibody for CD31 and DAPI followed. Images were then taken on an Olympus FV1000 confocal microscope.

Results

Establishment of rat liver metastasis model with syngeneic rat colon carcinoma cells

We established the CC531 colorectal rat metastasis model in our laboratory in order to have a relevant animal model in which to study imaging of hepatic metastasis. A rat model (WAG/RijHsd) was established for investigating the production of hepatic metastases by CC531 syngeneic rat colon carcinoma cells. Rats were anesthetized and the abdomen was opened, and then CC531 cells (2×10^6) suspended in 0.2 mL of phosphate-buffered saline (PBS) were directly injected into the spleen. 2–4 weeks after intrasplenic injection of CC531 cells, the rats were inspected by midline incision. The tumors in the liver reached 1–2 mm in diameter four weeks after intrasplenic injection (Figure 1).

NIH-PA Author Manuscript

NIH-PA Author Manuscript

NIH-PA Author Manuscript

Photostability of Eu-G3P418N

Due to the presence of the lanthanide cations, the luminescent compound is predicted to be resistant to photobleaching. To examine this possibility, the fluorescence from the 1,8-naphthalimide derivative was monitored as a function of time upon exposure to excitation light (Figure 3D). In the absence of Eu^{3+}, the signal intensity increased for the first thirty seconds but gradually decreased for the remainder of the experiment. This behavior indicates that the complex is subject to photobleaching. However, the photophysical properties of Eu-G3P4A18N dendrimer are different (Figure 3D). In the presence of Eu^{3+}, the signal intensity increased during the first thirty seconds, and continuously increased and then maintained at a constant value. These data suggest that Eu^{3+} appears to stabilize the thirty-two 1,8-naphthalimide chromophores against photobleaching.

Multiple tumor imaging with Eu-G3P4A18N

Multiple metastatic tumor nodules were generated in a rat liver via a splenic injection of CC531 colorectal cancer cells. After infusion of Eu-G3P4A18N via the GDA cannulation technique, the rat liver was excised and imaged by luminescence. Figure 4A shows the gross and corresponding luminescence images of *ex vivo* livers after being infused with a volume of 300 μL of a 60 μM solution of Eu^{3+} only, generation 3 PAMAM (G3P) dendrimer only, or Eu-G3P4A18N in 10% DMSO/H_2O (Figure 4A a–c and a′–c′). To identify the luminescent signal in the liver and tumor tissue, tissue slices were examined with a confocal microscope (Figure 4A a″–c″). Photograph (a) describes a control liver that was infused with Eu^{3+} (europium only) and showed no luminescence in any of the corresponding photographs (a′ or a″). Photograph (b) shows another control liver that was infused with G3P dendrimer and very little to no luminescence was observed in either photograph (b′ or b″). Photograph (c) shows the experimental liver that was infused with Eu-G3P4A18N and does show luminescence to be present in the corresponding tumors in photograph (c′) and (c″). Figure 4B shows the relative fluorescence signal that was observed in all three experiments. It demonstrates that the luminescence in the Eu-G3P4A18N infused liver was brighter than that of the controls. Although the fluorescence signal does not penetrate through all the tissue, our data demonstrate that the metastatic nodules display a more intense luminescence signal than either the background or the controls after infusion with Eu-G3P4A18N.

Retention time of the Eu-G3P4A18N in tumors

To determine the retention time of the dendrimer in the tumor post infusion, rats were injected intrahepatically via the GDA with Eu-G3P4A18N and sacrificed at the following time points: 0 hour, 4 hours, 24 hours, 72 hours and 5 days (Figure 5A). Sustained luminescence signals from the tumors were observed at all time points post infusion as well as an increase in luminescence signal intensity over time (Figure 5A a′ – e′). The corresponding confocal microscopic images, which identified the Eu-G3P4A18N in the liver and tumor tissue, also demonstrate the uptake of the Eu-G3P4A18N in the hepatic nodules (Figure 5A a″ – e″). Background autofluorescence of the liver was accounted for and the resulting bar graph (Figure 5B) demonstrates that luminescence signals from the tumors were present up to 5 days post infusion with Eu-G3P4A18N. It also describes a correlation between signal intensity and time.

Selective tumor targeting by Eu-G3P4A18N

Confocal microscopy helps to identify the location which the Eu-G3P4A18N targets. Figure 6 demonstrates, in a 20× magnified confocal microscopic image, that the uptake of Eu-G3P4A18N is apparent on the tumor section of a liver (left of the white line) and not found in the normal liver parenchyma (right of the white line) 24 hours after it was infused. The

NIH-PA Author Manuscript

NIH-PA Author Manuscript

NIH-PA Author Manuscript

luminescence of the Eu-G3P4A18N is depicted by the arrows and to the left of the white line.

Discussion

We have demonstrated, by way of cannulating the GDA, that we can deliver a novel PAMAM dendrimer targeting system into the liver of rats. We have been able to use a clinically relevant colorectal metastases model, and through isolated hepatic perfusion, have localized the tumors by way of luminescence imaging. We have taken advantage of a disorganized tumor vasculature and been able to deliver our approximately 3 nm sized dendrimer through the widened inter-endothelial junctions and fenestrae that range from 400 to 800 nm in size21, since tumor vasculature is “leaky” and allows larger molecules to extravasate the vascular endothelium into the extravascular space and in the process bypass normal liver parenchyma. The relatively small size of our dendrimer22 facilitates its exit through the fenestrae and allows it to be trapped in the extravascular spaces of the tumor. The confocal microscopy observations are consistent with the hypothesis that Eu-G3P4A18N has increased extravasation from the leaky tumor vasculature and, therefore, is more likely to be trapped in the perivascular spaces of the tumor. This is believed to provide us with the immediate luminescence that is observed at the 0 hour time point. However, it is also observed that an accumulation or an increase of luminescence intensity is seen after 24 hours. This could probably be due to a movement of Eu-G3P4A18N from the immediate perivascular space into more distal areas of the tumor.

Metastasis to the liver from colorectal cancer is what decreases survival rates and is therefore an appropriate focus for therapeutic strategies requiring hepatic infusion. Any animal model designed to study hepatic infusion must mimic the clinical setting through (1) employing an adenocarcinoma cell type, (2) using vascular access which is used in the clinical setting of regional therapies, and (3) being able to undergo multiple surgeries. An additional advantage of this model is that the CC531 rat tumor model has been used for studies which include TACE and laser-induced therapy for treatment of liver metastases, but utilized a subcapsular tumor cell injection in contrast to the splenic injection technique described. Splenic injections and metastases to the liver provide for better imaging applications to be studied and more importantly, it is a better clinical model. The combination of the hepatic colorectal metastatic model and the GDA cannulation technique provides a model which reflects isolated hepatic perfusion performed on humans[23] and [24] and can also be implemented to study treatments which include hyperthermia combined with chemotherapeutics. Treatments that are currently in place for hepatic metastatic disease have led to only slight improvement in survival rates over the years, but that has only come from using different combinations of regional chemotherapies, surgical resection, RFA or isolated hepatic perfusion. These treatments can be enhanced to become more effective clinically when combined with new innovative treatment strategies that are currently underway in the laboratory setting.

Polyamidoamine (PAMAM) dendrimers are biocompatible,17 nonimmunogenic,18 and water soluble and have been attached to metals[16] and [25] as well as many biological molecules such as antibodies, synthetic drugs, and small molecules.[14], [15], and [26] Previous studies reveal that dendrimers can be used as multifunctional carriers capable of combining targeted drug delivery and imaging in pharmaceutical applications.[13] and [27] In this study, we introduced the use of novel dendrimers that incorporate a core constituted of generation-3 PAMAM with terminal branch modifications. Europium ions are incorporated into the dendrimer to stabilize it for its use as an imaging agent. The dendrimer compounds provide improved detection in biological media because of their near infrared (NIR) emission (lower autofluorescence in this energy domain). Biological tissues do not

NIH-PA Author Manuscript

NIH-PA Author Manuscript

NIH-PA Author Manuscript

have significant NIR luminescence. Therefore, use of NIR eliminates background fluorescence, one of the most important issues for biological imaging. However, the disadvantage of this approach is that fluorescent signal does not penetrating through all the tissue and therefore is not quantitative.

Our studies demonstrate that our modified dendrimer preferentially accumulated in metastatic tumors and had a long retention time. In future studies, we will take advantage of these observations for developing a novel nanotechnology therapy in combination with conventional therapy. As an example, we believe that this dendrimer can serve as a target for a non-invasive low power radiofrequency (RF) field which in turn releases heat to generate localized hyperthermia. This idea is based on previous observations that europium ion-cored dendrimers are excellent conductors of electrical and thermal energy and can be used as thermal conductors of non-invasive low power radiofrequency ablation to generate hyperthermia. Previous studies reveal that hyperthermia acts synergistically with ionizing radiation,[28], [29], and [30] with a number of chemotherapeutic agents,[31], [32], and [33] and with various cytokines.[34], [35], and [36] We believe that the multimodality approach with hyperthermia + radiation + chemotherapeutic agent + cytokine will improve the treatment against metastasized hepatic colorectal cancer.

In order to further drive clinical improvements, investigation of mechanisms of TACE therapy can be better understood utilizing our animal model. Radiofrequency ablation utilizing a probe inserted into the liver has a role in the therapy for liver metastasis. However, it can potentially play a larger role based on the animal model described here. This would avoid surgery altogether as described by Gannon et al.[37] and [38] Tumor targeting is a problem for most researchers, but it, too, can be investigated closely in the animal model. The importance of a reliable tumor model system, coupled with an unambiguous method for isolated perfusion which mimics the clinical setting, is the enabling of preclinical development and the evaluation of new approaches and technologies for regional therapies. This preclinical development will result in facile translation for positive clinical impact for patients with hepatic metastases of colorectal cancer.

Acknowledgments

We thank Per Basse, M.D., Ph.D., DMSci for making available the CC531 colorectal cancer cells.

Funding sources: The original studies in the authors' laboratories were funded in part by grants from the David C. Koch Therapy Cancer Center, the National Institute of Health T32 CA113263 (DLB) “Postdoctoral Research Training in Biotherapy of Cancer” grant, R01GM066018 (MW and SGW) and R01CA140554 (YJL). Stéphane Petoud aknowledge support from the National Institute of Health 1R21CA133553, from la Ligue contre le Cancer and from Institut National de la Santé et de la Recherche Médicale (INSERM).

ABBREVIATIONS

CCD	charge coupled device
DIPEA	*N*,*N*-Diisopropylethylamine
DMEM	Dulbecco's modified Eagle's medium
DMF	dimethylformamide
DMSO	Dimethyl sulfoxide
Eu	europium
G3P4A18N	generation 3 polyamidoamine 4-amino-1,8-naphthalimide
GDA	gastroduodenal artery

NIH-PA Author Manuscript

NIH-PA Author Manuscript

NIH-PA Author Manuscript

HATU	2-(1H7-7-Azabenzotriazol-1-yl)-1,1,3,3-tetramethyl uranium hexafluorophosphate Methanaminium
MWCO	molecular weight cut-off
NIR	near infrared
NMR	nuclear magnetic resonance
PAMAM	polyamidoamine
PBS	phosphate-buffered saline
RT	regional therapy
TACE	transarterial chemoembolization
TLC	thin layer chromatography

References

1. Jemal A, Siege R, Ward E, Hao Y, Xu J, Murray T, et al. Cancer statistics. Cancer J Clin. 2008; 58:71–96. 2008. CA.
2. Park, JO.; Brown, CK. Colorectal cancer. In: Brown, CK.; Rini, BI.; Connell, PP.; Posner, MC., editors. Holland - Frei manual of cancer medicine. BC Decker Inc; Hamilton: 2005. p. 184-204.
3. Abdalla EK, Vauthey J-N, Ellis LM, Ellis V, Pollock R, Broglio KR, et al. Recurrence and outcomes following hepatic resection, radiofrequency ablation, and combined resection/ablation for colorectal liver metastases. Ann Surg. 2004; 239:818–827. [PubMed: 15166961]
4. Kemeny N, Huang Y, Cohen AM, Shi W, Conti JA, Brennan MF, et al. Hepatic arterial infusion of chemotherapy after resection of hepatic metastases from colorectal cancer. New Engl J Med. 1999; 341:2039–2048. [PubMed: 10615075]
5. Duijnhoven FH, Tollenaar RAEM, Terpstra OT, Kuppen PJK. Locoregional therapies of liver metastases in a rat CC531 coloncarcinoma model results in increased resistance to tumour rechallenge. Clin Exp Metastasis. 2005; 22:247–253. [PubMed: 16158252]
6. Maataoui A, Qian J, Mack MG, Khan MF, Oppermann E, Roozru M, et al. Liver metastases in rats: chemoembolization combined with interstitial laser ablation for treatment. Radiology. 2005; 237:479–484. [PubMed: 16244257]
7. Thomas C, Nijenhuis AM, Timens W, Kuppen PJ, Daemen T, Scherphof GL. Liver metastasis model of colon cancer in the rat: immunohistochemical characterization. Invasion Metastasis. 1993; 13:102–112. [PubMed: 8225852]
8. Gupta S, Kobayashi S, Phongkitkarun S, Broemeling LD, Kan Z. Effect of transcatheter hepatic arterial embolization on angiogenesis in an animal model. Invest Radiol. 2006; 41:516–521. [PubMed: 16763470]
9. Masyuk TV, Ritman EL, LaRusso NF. Hepatic artery and portal vein remodeling in rat liver: vascular response to selective cholangiocyte proliferation. Am J Pathol. 2003; 162:1175–1182. [PubMed: 12651609]
10. Li X, Wang Y-XJ, Zhou X, Guan Y, Tang C. Catheterization of the hepatic artery via the left common carotid artery in rats. Cardiovasc Intervent Radiol. 2006; 29:1073–1076. [PubMed: 16670846]
11. Wittmer A, Khazaie K, Berger MR. Quantitative detection of lac-Z-transfected CC531 colon carcinoma cells in an orthotopic rat liver metastasis model. Clin Exp Metastasis. 1999; 17:369–376. [PubMed: 10651303]
12. Kollmar O, Schilling MK, Menger MD. Experimental liver metastasis: standards for local cell implantation to study isolated tumor growth in mice. Clin Exp Metastasis. 2004; 21:453–460. [PubMed: 15672870]
13. Cheng Y, Wang J, Rao T, He X, Xu T. Pharmaceutical applications of dendrimers: promising nanocarriers for drug delivery. Front Biosci. 2008; 13:1447–1471. [PubMed: 17981642]

NIH-PA Author Manuscript NIH-PA Author Manuscript NIH-PA Author Manuscript

14. Patri AK, Kukowska-Latallo JF, Baker JR Jr. Targeted drug delivery with dendrimers: comparison of the release kinetics of covalently conjugated drug and non-covalent drug inclusion complex. Adv Drug Del Rev. 2005; 57:2203–2214.
15. Patri AK, Majoros IJ, Baker JR Jr. Dendritic polymer macromolecular carriers for drug delivery. Curr Opin Chem Biol. 2002; 6:466–471. [PubMed: 12133722]
16. Kaczorowska MA, Cooper HJ. Electron capture dissociation and collision-induced dissociation of metal ion (Ag^{+}, Cu^{2+}, Zn^{2+}, Fe^{2+}, and Fe^{3+}) complexes of polyamidoamine (PAMAM) dendrimers. J Am Soc Mass Spectrom. 2009; 20:674–681. [PubMed: 19196522]
17. Duncan R, Izzo L. Dendrimer biocompatibility and toxicity. Adv Drug Del Rev. 2005; 57:2215–2237.
18. Roberts JC, Bhalgat MK, Zera RT. Preliminary biological evaluation of polyamidoamine (PAMAM) Starburst dendrimers. J Biomed Mater Res. 1996; 30:53–65. [PubMed: 8788106]
19. Yuan D, Brown RG, Hepworth JD, Alexiou MS, Tyman JHP. The synthesis and fluorescence of novel *N*-substituted-1,8-naphthylimides. J Heterocycl Chem. 2008; 45:397–404.
20. Cross JP, Lauz M, Badger PD, Petoud S. Polymetallic lanthanide complexes with PAMAM-naphthalimide dendritic ligands: luminescent lanthanide complexes formed in solution. J Am Chem Soc. 2004; 126:16278–16279. [PubMed: 15600302]
21. Svenson S, Tomalia DA. Dendrimers in biomedical applications-reflections on the field. Adv Drug Del Rev. 2005; 57:2106–2129.
22. Maiti PK, Çagin T, Wang G, Goddard WA III. Structure of PAMAM dendrimers: generations 1 through 11. Macromolecules. 2004; 37:6236–6254.
23. Bartlett DL, Libutti SK, Figg WD, Fraker DL, Alexander HR. Isolated hepatic perfusion for unresectable hepatic metastases from colorectal cancer. Surgery. 2001; 129:176–187. [PubMed: 11174711]
24. Alexander HR, Libutti S, Pingpank J, Bartlett D, Helsabeck C, Beresneva T. Isolated hepatic perfusion for the treatment of patients with colorectal cancer liver metastases after irinotecan-based therapy. Ann Surg Oncol. 2005; 12:138–144. [PubMed: 15827794]
25. Newkome GR, Shreiner CD. Poly(amidoamine),polypropylenimine, and related dendrimers and dendrons possessing different 1-> 2 branching mofits: An overview of the divergernt procedures. Polymer. 2008; 49:1–173.
26. Shukla R, Thomas TP, Peters JL, Desai AM, Kukowska-Latallo J, Patri AK, et al. HER2 Specific tumor targeting with dendrimer conjugated anti-HER2 mAb. Bioconj Chem. 2006; 17:1109–1115.
27. Matsuura N, Rowlands JA. Towards new functional nanostructures for medical imaging. Med Phys. 2008; 35:4474–4487. [PubMed: 18975695]
28. Dewey WC, Sapareto SA, Betten DA. Hyperthermic radiosensitization of synchronous chinese hamster cells: relationship between lethality and chromosomal aberrations. Radiat Res. 1978; 76:48–59. [PubMed: 569879]
29. Holahan EV, Highfield DP, Holahan PK, Dewey WC. Hyperthermic killing and hyperthermic radiosensitization in chinese hamster ovary cells: effects of pH and thermal tolerance. Radiat Res. 1984; 97:108–131. [PubMed: 6695037]
30. Kampinga HH, Dikomey E. Hyperthermic radiosensitization: mode of action and clinical relevance. Int J Radiat Biol. 2001; 77:399–408. [PubMed: 11304434]
31. Haas GP, Klugo RC, Hetzel FW, Barton EE, Cerny JC. The synergistic effect of hyperthermia and chemotherapy on murine transitional cell carcinoma. J Urol. 1984; 132:828–833. [PubMed: 6540817]
32. Herman TS, Sweets CC, White DM, Gerner EW. Effect of heating on lethality due to hyperthermia and selected chemotherapeutic drugs. J Natl Cancer Inst. 1982; 68:487–491. [PubMed: 6950177]
33. Ko SH, Ueno T, Yoshimoto Y, Yoo JS, Abdel-Wahab OI, Abdel-Wahab Z, et al. Optimizing a novel regional chemotherapeutic agent against melanoma: hyperthermia-induced enhancement of temozolomide cytotoxicity. Clin Cancer Res. 2006; 12:289–297. [PubMed: 16397054]
34. Klostergaard J, Leroux E, Siddik ZH, Khodadadian M, Tomasovic SP. Enhanced sensitivity of human colon tumor cell lines in vitro in response to thermochemoimmunotherapy. Cancer Res. 1992; 52:5271–5277. [PubMed: 1394131]

NIH-PA Author Manuscript

NIH-PA Author Manuscript

NIH-PA Author Manuscript

35. Lee YJ, Hou Z, Curetty L, Cho JM, Corry PM. Synergistic effects of cytokine and hyperthermia on cytotoxicity in HT-29 cells are not mediated by alteration of induced protein levels. J Cell Physiol. 1993; 155:27–35. [PubMed: 8468367]

36. Srinivasan JM, Fajardo LF, Hahn GM. Mechanism of antitumor activity of tumor necrosis factor α with hyperthermia in a tumor necrosis Factor α-resistant tumor. J Natl Cancer Inst. 1990; 82:1904–1910. [PubMed: 2250311]

37. Gannon CJ, Chaerukuri P, Yakobson BI, Cognet L, Kanzius JS, Kittrell C, et al. Carbon nanotube-enhanced thermal destruction of cancer cells in a noninvasive radiofrequency field. Cancer. 2007; 110:2654–2665. [PubMed: 17960610]

38. Gannon CJ, Patra CR, Bhattacharya R, Mukherjee P, Curley SA. Intracellular gold nanoparticles enhance non-invasive radiofrequency thermal destruction of human gastrointestinal cancer cells. J Nanobiotechnol. 2008; 6:2.

NIH-PA Author Manuscript

NIH-PA Author Manuscript

NIH-PA Author Manuscript

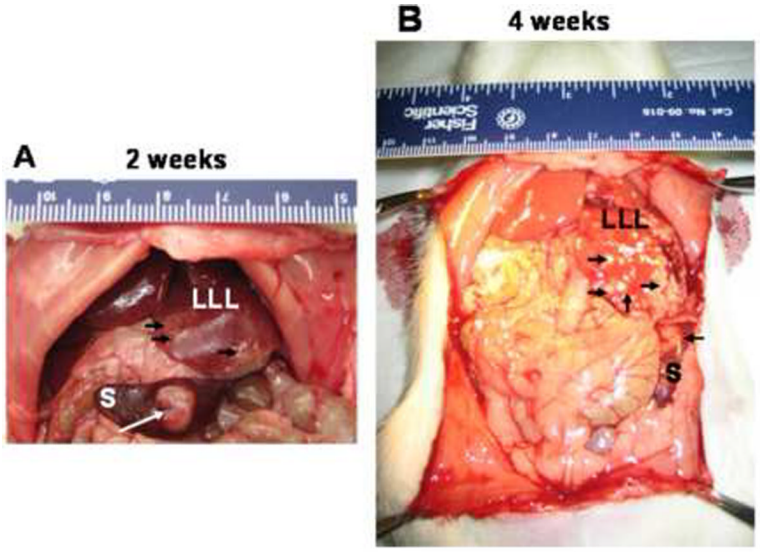

Figure 1. Tumorigenicity and metastasis of CC531 cells in WAG/RijHsd rats

Syngeneic rat colon carcinoma CC531 cells (2×10^6 cells in 0.2 ml of PBS) were injected into the spleen of rats and tumor formation was observed after 2 weeks **(A)** or 4 weeks **(B).** Tumors were observed in the spleen (S) and the left lateral lobe (LLL). Arrows point out the location of tumors.

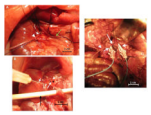

Figure 2. GDA cannulation technique

Photograph **(A)** shows the inferior aspect of the liver showing the silk sutures around the hepatic artery (long arrow), portal vein (green long arrow), proximal and distal ends of the GDA (short arrow) and the catheter placed into the GDA (arrowhead). **(B)** shows a 30 gauge needle (short arrow) being used as a hook for control when inserting the catheter into the GDA (long arrow); arrowhead indicates the hepatic artery; a swab is shown at the bottom (black arrow) so as to display the vascular network and photograph. **(C)** shows the placement of the PE-10 catheter (arrowhead) cannulated into the GDA and anchored down with a silk suture (long arrow) and the two vascular clamps (short arrows) on the portal vein and the hepatic artery.

NIH-PA Author Manuscript
NIH-PA Author Manuscript
NIH-PA Author Manuscript

NIH-PA Author Manuscript
NIH-PA Author Manuscript
NIH-PA Author Manuscript

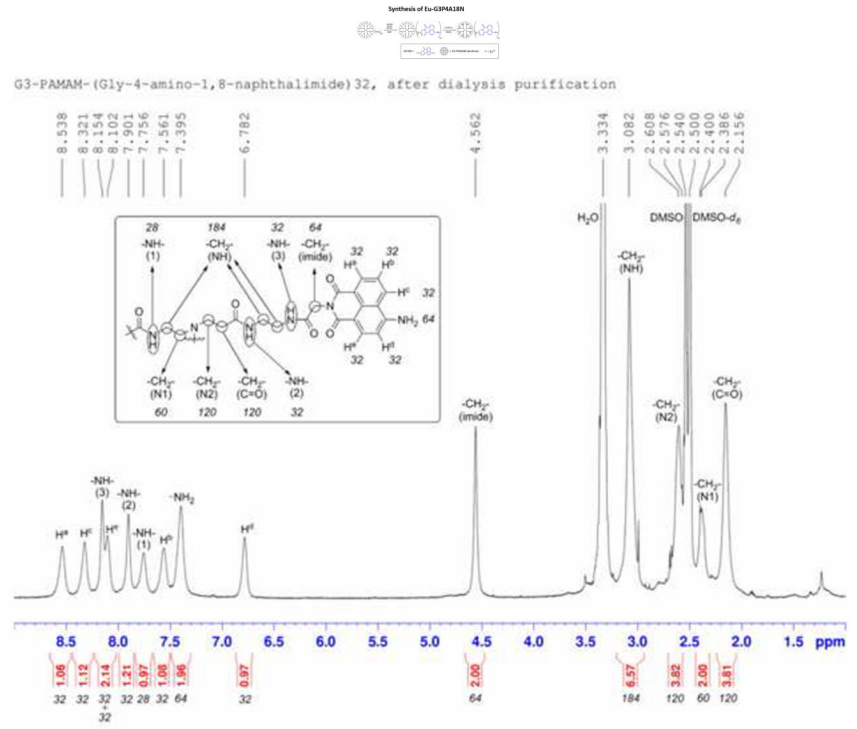

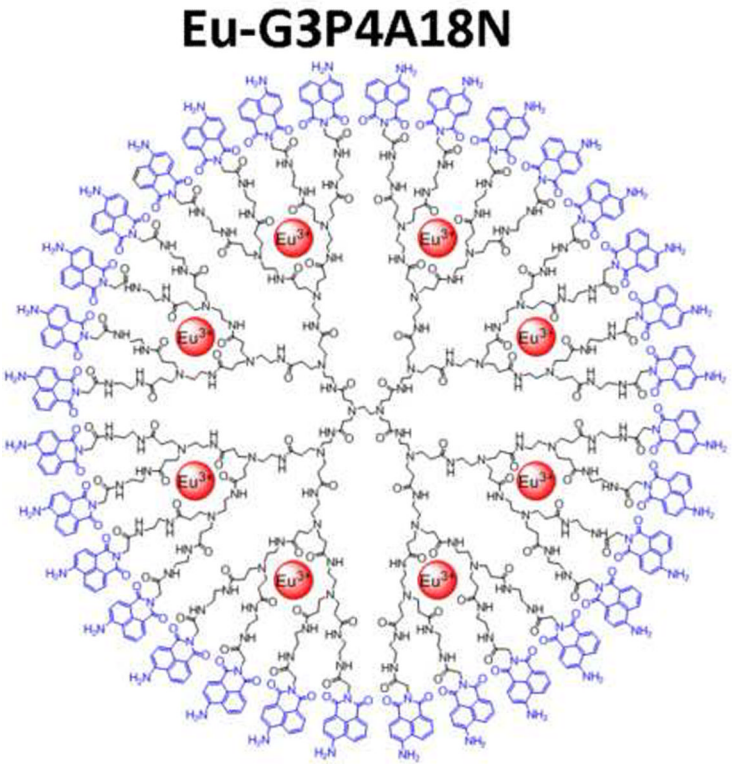

NIH-PA Author Manuscript

NIH-PA Author Manuscript

NIH-PA Author Manuscript

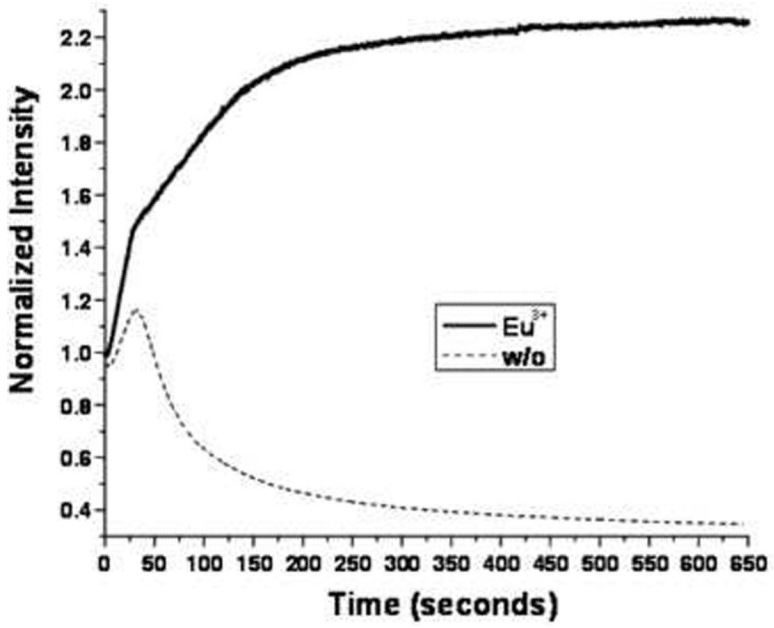

Figure 3. Synthesis, characterization and structure of Eu-G3P4A18N

(A) Synthetic scheme of Eu-G3P4A18N. (**B**) Characterization of G3P4A18N by NMR. **(C)** Structure of Eu-G3P4A18N, which contains thirty-two 4-amino-1,8-naphthalimide units and eight europium cations. (**D**) Photobleaching analysis of Eu-G3P4A18N dendrimer. The fluorescence from the 1,8 naphthalimide derivative was monitored as a function of time upon exposure to excitation light.

NIH-PA Author Manuscript

NIH-PA Author Manuscript

NIH-PA Author Manuscript

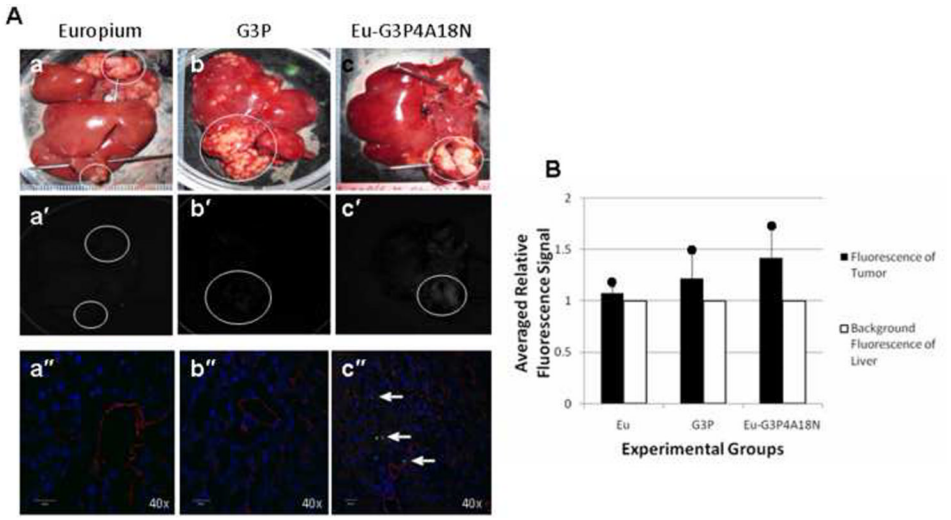

Figure 4. ***In vivo*** **cannulation with Eu^{3+}, G3P and Eu-G3P4A18N with luminescence imaging and analysis**

(A) Gross photographs, luminescence and confocal microscopic images at 40× magnification of the livers containing tumors (circles) that were injected in the spleen 15–20 days prior to infusion and excised at 0 h time point. Photos (a), (a′) and (a″) were from infusion of Eu^{3+} only at 0 h. Photos (b), (b′) and (b″) were from infusion of G3P (non-functionalized dendrimer without Eu^{3+}) and at 0 h. Photos (c), (c′) and (c″) were from liver infused with Eu-G3P4A18N at 0 h. Arrows show the luminescence of Eu-G3P4A18N in the confocal microscopic images in photo (c″). **(B)** Average tumor luminescence was corrected for background autofluorescence in the resulting graph. Two rats per each experimental group were used.

NIH-PA Author Manuscript

NIH-PA Author Manuscript

NIH-PA Author Manuscript

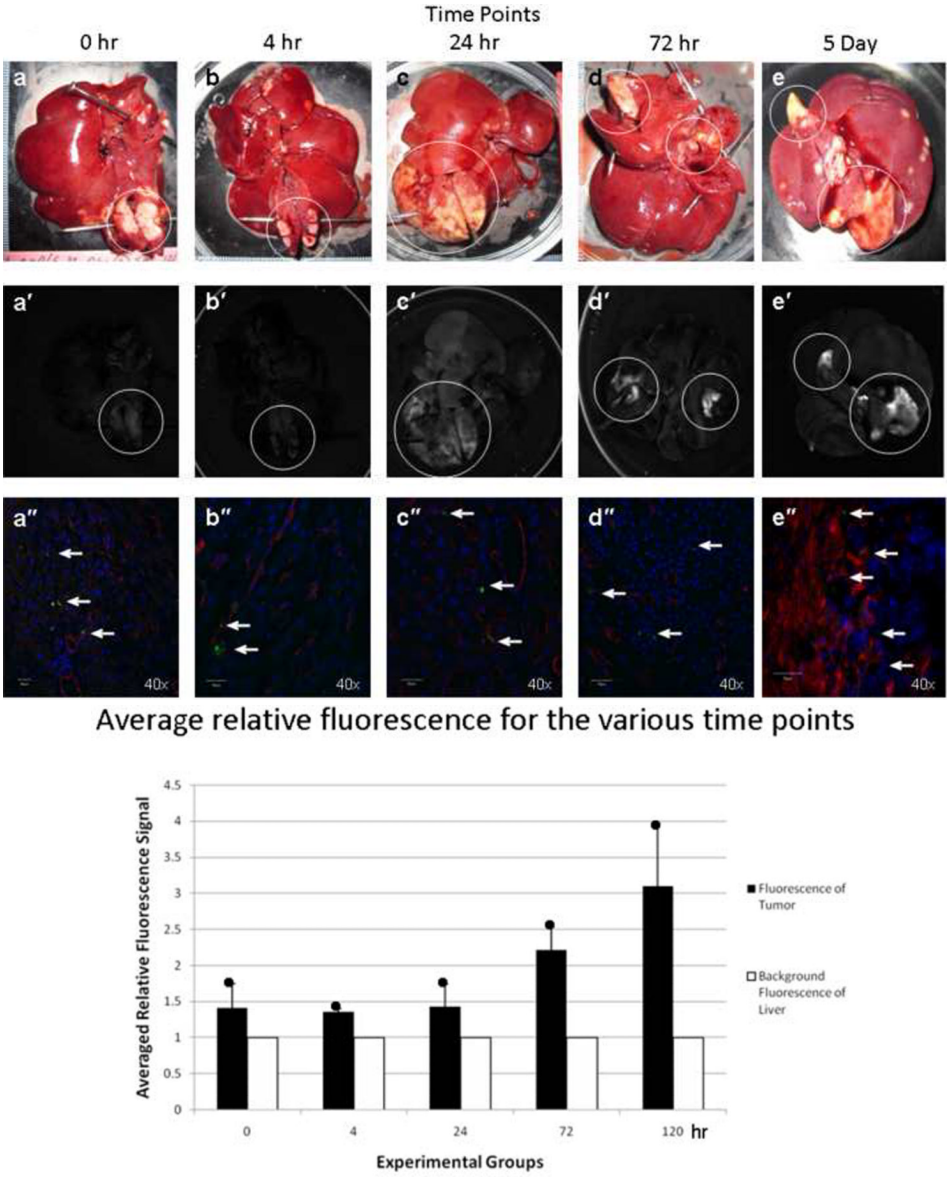

Figure 5. ***In vivo h*epatic infusions with Eu-G3P4A18N over several time points with analysis of the tumor luminescence**

(A) Gross photographs of the livers containing tumors (circles) that were injected in the spleen 15 – 20 days prior to infusion of Eu-G3P4A18N and excised at 0 h, 4 h, 24 h, 72 h and 5 day time points (a – e). Images (a′ – e′) were from the same liver and tumor tissue and same hepatic infusions with Eu-G3P4A18N under fluorescence imaging displaying grossly the tumor luminescence. 40× magnifications of confocal microscopic images (a″ – e″) were also obtained from the same liver and tumor tissue and same corresponding time points displaying luminescence signaling in all time points (arrows). **(B)** Average signals obtained from the tumors were compared to that of tissue autofluorescence and displayed in the resulting graph. Two rats per each experimental group were used.

NIH-PA Author Manuscript

NIH-PA Author Manuscript

NIH-PA Author Manuscript

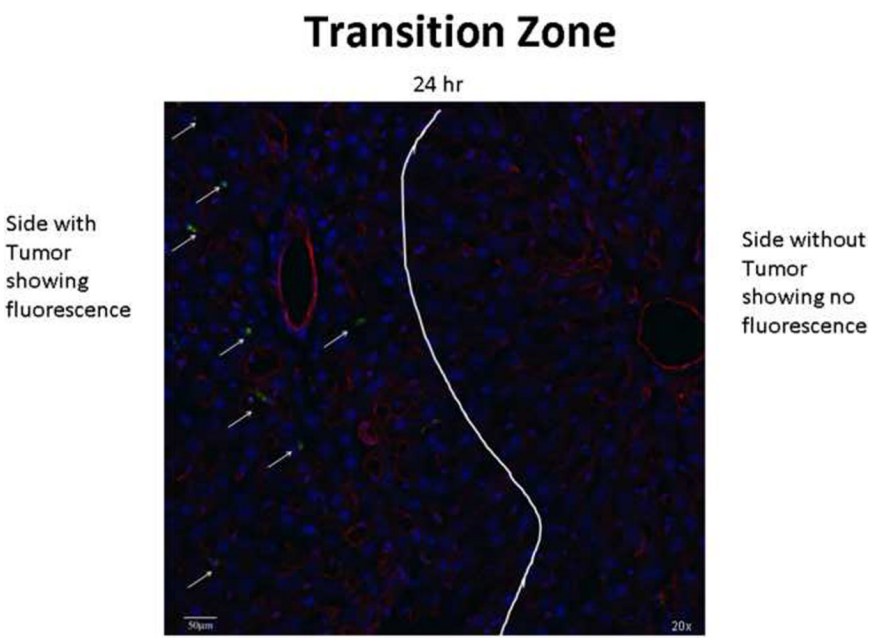

Figure 6. Transition zone between normal liver and tumor

A 20× confocal microscopic image of a rat liver containing a metastatic tumor which was infused with Eu-G3P4A18N and then the liver was excised 24 h later. The transition zone between the healthy normal liver (right of the white line) and the tumor (left of the white line) is seen. The arrows point to the green luminescence given off from the Eu-G3P4A18N itself and it is not seen on the healthy liver side.